Available online at www.sciencedirect.com

ScienceDirect

Ceramics International 40 (2014) 2677–2684

CERAMICS INTERNATIONAL

www.elsevier.com/locate/ceramint

Dopant induced RTFM and enhancement of fluorescence efficiencies in spintronic ZnS:Ni nanoparticles

B. Poornaprakash[a], S. Sambasivam[b], D. Amaranatha Reddy[a,c], G. Murali[a], R.P. Vijayalakshmi[a], B.K. Reddy[a,*]

[a]Department of Physics, Sri Venkateswara University, Tirupati 517502, India
[b]Department of Physics, Pukyong National University, Busan, South Korea
[c]Department of Physics, Hankuk University of foreign studies, Yongin, Korea

Received 13 September 2013; received in revised form 10 October 2013; accepted 11 October 2013
Available online 21 October 2013

Abstract

Diluted magnetic semiconducting (DMS) ZnS:Ni (Ni = 0, 1, 3 and 5 at%) nanoparticles were synthesized by the refluxing technique at 80 °C. X-ray diffraction studies showed that undoped ZnS and Ni doped ZnS nanoparticles exhibited the expected zinc blende structure. X-ray photoelectron spectroscopy results revealed that the Ni ions existed in a +2 state in these nanoparticles. Reflectance measurements showed a decrease in band gap with increasing Ni concentration. Room temperature photoluminescence (PL) studies indicated that all the samples exhibited broad and asymmetric PL peaks covering a wide visible range. Gaussian fitting of PL data resulted in three deconvoluted peaks corresponding to blue and green emissions. Dramatic enhancement in fluorescence efficiency was observed in the doped ZnS nanoparticles indicating their possible applications in photoluminescent devices. Magnetic studies revealed that all the doped samples exhibited carrier mediated ferromagnetism at room temperature. Saturation magnetization (M_s) increased with increasing Ni content reaching a maximum for 3 at% Ni and decreased for samples of 5 at% Ni.

Keywords: Nanoparticles; Photoluminescence; Room temperature ferromagnetism

1. Introduction

Recently, research on nanoscience has become quite popular in various fields of chemistry and physics and the technology of production of nanostructures and their use is rapidly growing into a powerful industry. Among the various important categories of functional materials, diluted magnetic semiconductors (DMS), with the charge and spin degrees of freedom of the charge carriers accommodated into a single material have emerged as novel materials and have attracted considerable attention. Nanoscale diluted magnetic semiconductors, displaying interesting magnetic, magneto optical and magneto electrical properties [1,2] due to large surface area to volume ratio referred to as specific surface area (SSA), form the main components of spintronic devices. DMS are obtained by doping transition or rare earth metal ions into non-magnetic semiconductors. These ions have partially filled d and f shells which give rise to unpaired electrons leading to magnetism in the DMS materials. In spite of a number of papers published [3–6], the situation is far from being well understood and there is no clear agreement about the origin of the magnetic behavior observed in DMS materials. The ferromagnetism detected in most cases was earlier attributed [7,8] to extrinsic effects such as ferromagnetic precipitates and impurity phases. The present day challenge is to look for modified semiconductors which exhibit stable and intrinsic ferromagnetism at room temperature for use in the new generation spintronic devices. As an important II–VI semiconducting compound, ZnS is chemically more stable, inexpensive, environmentally safe, technologically better than other chalcogenides and is a good host for most of the transition or rare earth metal ion dopants and is

*Corresponding author. Tel.: +91 94 40324223.
E-mail addresses: yoursborrak@gmail.com, borrak2001@yahoomail.com (B.K. Reddy).

0272-8842/$ - see front matter © 2013 Elsevier Ltd and Techna Group S.r.l. All rights reserved.
http://dx.doi.org/10.1016/j.ceramint.2013.10.056

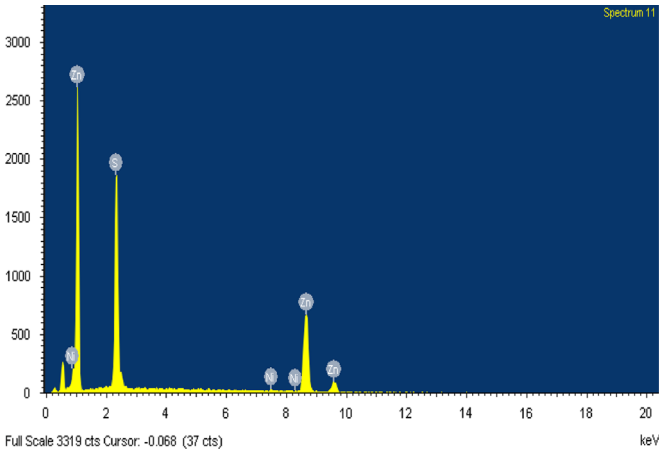

Fig. 1. EDAX spectra of ZnS:Ni (3 at%) nanoparticles.

known to exhibit remarkable optical and magnetic properties [9–11]. ZnS based magnetic semiconductors with similar crystal structure and matching lattice parameters [12] are the most preferred candidates for investigation for application in the main stream silicon technology. Remarkably, a number of investigators have demonstrated ferromagnetism with Curie temperature above room temperature in transition metal doped ZnS nanoparticles [3,4,13,14]. Generally, the tunability of the properties of nanoparticles by controlling their size may provide an advantage in formulating new composite materials with optimized properties for various applications. However, these may be restricted by different non-radiative relaxation path ways like surface related defects. Such difficulties may be overcome by using organic or inorganic stabilizers to passivate the free quantum dots. Polyvinyl pyrrolidone (PVP), polyvinyl alcohol (PVA), polyethylene glycol (PEG), ethylene diamine tetra acetic acid (EDTA), thioacetamide (TAA) etc. are generally used as surfactants. Tunable optical and magnetic properties may be achieved by judiciously choosing the dopants and their concentrations. Earlier workers have reported the effect of dopants like Mn [9], Cu [10], Cr [11], Fe [13] on the optical and magnetic properties of ZnS nanoparticles. To the best of our knowledge, there is only one report on the magnetic properties of Ni doped ZnS [14]. Nickel is ferromagnetic, a reasonable conductor of heat and electricity and is corrosion resistant. Further, Ni^{2+} has an ionic radius of 0.69 Å which is smaller than that of Zn^{2+} (0.74 Å) and hence Ni^{2+} can easily replace Zn^{2+} in ZnS host lattice. This has motivated the present authors to undertake this investigation. In the present study systematic investigations, on the structural, optical and magnetic properties of Ni doped ZnS nanoparticles synthesized by the chemical route, have been carried out and the results are reported in this paper.

2. Experimental

ZnS:Ni (Ni = 0, 1, 3 and 5 at%) nanoparticles were synthesized by the refluxing method at 80 °C using PVP as capping agent. Zinc acetate dehydrate, nickel chloride and sodium sulfide were used as precursors. In a typical procedure, 0.2 M zinc acetate and required amount of nickel chloride were mixed with 50 ml of methanol and stirred for 30 min. Separately prepared solution of sodium sulfide was added drop by drop to this mixture. Finally, an appropriate amount of PVP was added to the above solution as a capping agent. The mixture was refluxed for 3 h at a temperature of 80 °C. The solution obtained was filtered, washed with ethanol and water many times to remove the impurities and was dried in an oven at 80 °C for 8 h.

Chemical analysis was carried out using a CARL ZEISS EVO MA15, Scanning Electron Microscope (SEM) with an EDAX attachment. Structural studies on ZnS:Ni nanoparticles were done using a 'Seifert 3003TT X-ray diffractometer with Cu-Kα radiation with a wavelength of 1.540 Å and the system was operated at 30 KeV in the scan range of 20–70°. The particle size confirmation was done using a Phillips TECHNAI FE 12, Transmission Electron Microscope (TEM). Diffuse reflectance measurements were carried out on the synthesized nanopowders using a Jasco V-670 double-beam spectrometer for energy gap determination. PL emission spectra were recorded using OBIN YUON Fluorolog-3 spectrometer with a 450 W Xenon arc lamp as an excitation source. Magnetization was studied at room temperature using a VSM 7410 Lakeshore Vibrating Sample Magnetometer. A SPECS GmbH (Phoibos 100 MCD Energy Analyzer) X-ray Photon Spectrometer (XPS) with Al Kα radiation (1486.6 eV) with a residual pressure of the order of 2×10^{-8} Pa was used to check the presence of impurity phases in the samples.

3. Results and discussion

3.1. Elemental analysis

Fig. 1 depicts typical EDAX spectra for the undoped and nickel (3 at%) doped ZnS samples. The EDAX spectra exhibit signals corresponding to Zn, S and Ni only indicating that the nanoparticles are made up of zinc, sulfur and nickel only and no other impurity atoms within the detection limit of the instrument.

3.2. Structural analysis

The crystallinity and phase purity of the samples were investigated by X-ray diffraction (XRD) and TEM analysis. As shown in Fig. 2, the XRD patterns for Ni doped ZnS nanoparticles exhibit peak positions that match well with the standard pattern of zinc blende ZnS (JCPDS No. 05-0566). Absence of extra peaks indicates that no secondary phases or metal clusters are present in the samples within the detection limit of the instrument. The mean particle sizes in the Ni doped ZnS nanoparticles, estimated using the Debye–Scherrer formula from the major diffraction peak (111), lie in the range of 3–5 nm. The observed particle size decreases with increasing dopant concentration. Further, the peak positions shift towards higher 2θ values reflecting a decrease in lattice parameter with increasing Ni concentration and the estimated values of the lattice parameter are in the range of 5.42–5.39 Å. This could be due to the above mentioned decrease in particle

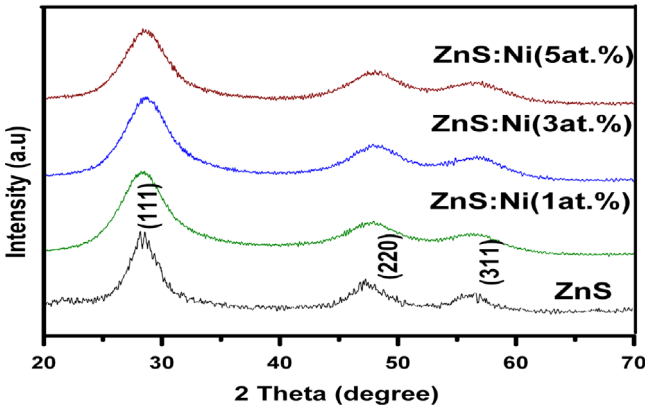

Fig. 2. XRD pattern of ZnS:Ni (0, 1, 3 and 5 at%) nanoparticles.

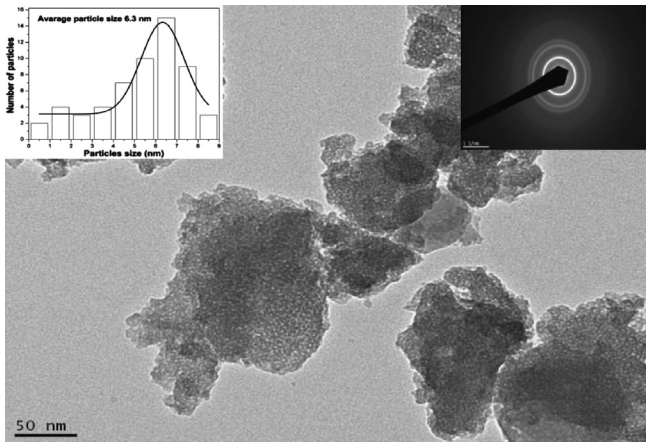

Fig. 3. TEM image of the ZnS:Ni (3 at%) nanoparticles with the insets showing the particle size distribution diagram (left) and SAED pattern (right).

size and also due to the smaller ionic radius of the substituting Ni^{2+} (0.69 Å) compared to that of Zn^{2+} (0.74 Å) of the host lattice. The corresponding TEM image (Fig. 3) reveals that the nickel doped ZnS nanoparticles are not ideally spherical. The estimated average particle size in the present samples is in the range of 5–10 nm. The values of the average particle size estimated from the XRD patterns are in the range of 3–5 nm. This disagreement between the TEM and XRD studies may be due to the fact that the crystallite size in fact can be larger than that predicted by the Scherrer formula with some extra peak width coming from micro strains which are most common in nanoparticles [15].

3.3. DRS analysis

Reflectance measurements on ZnS:Ni (Ni=0, 1, 3 and 5 at%) nanoparticles were done in the UV–visible region, 200–800 nm and the spectra are shown in Fig. 4(a). It may be noticed that the absorption edge of the samples shifts slightly to higher wavelengths with increasing dopant content. The band gaps of the samples were estimated from the diffuse reflectance spectra by plotting the square of the Kubelka–Munk [16] function $F(R)$ versus energy and extrapolating the linear part of the curve $F(R)^2=0$ as shown in Fig. 4(b). The values of band gap energy obtained for Ni doped ZnS are 3.92, 3.86, 3.80, and 3.76 eV for 0, 1, 3, and 5 at% Ni, respectively. This decrease in band gap with increase in dopant concentration may be due to the sp–d exchange interaction between the band electrons and the localized 'd' electrons of the Ni^{2+} ions substituting for the divalent Zn^{2+} ions [17–19]. Although some earlier researchers have reported [20–22] the optical properties of Ni doped ZnS nanoparticles, no mention of the band gap values has been made.

3.4. Photoluminescence studies

Fig. 5 illustrates the photoluminescence spectra of ZnS:Ni (Ni=0, 1, 3 and 5 at%) nanoparticles recorded at room temperature (300 K) using an excitation wavelength of 344 nm. All the samples exhibited broad and asymmetric PL peaks. The fluorescence efficiencies of the doped ZnS nanoparticles enhanced dramatically and are significantly higher (10 times) than those of the undoped ZnS nanoparticles. However, the intensity within the doped samples decreased with increase in doping concentration, the samples with 1 at% Ni exhibiting the maximum PL intensity. The PL intensity of the 5 at% Ni doped samples dropped below that of the undoped samples. The PL quenching may be due to increase in the non-radiative transitions at higher concentrations of the Ni^{2+} ions or due to concentration quenching effects [23]. This result implies that the optimum doping level of Ni^{2+} in ZnS for achieving maximum enhancement in PL intensity is around 1 at%. The present study indicates the possibility of application of these nanoparticles in luminescent devices.

The PL peaks of the present ZnS:Ni nanoparticles (Fig.5) are flat covering considerable wavelength region (390–550 nm) and indicate that they comprise different emission peaks. Gaussian fitting of PL data of undoped and doped samples deconvoluted into three small emission peaks as shown in Fig.6. In the undoped samples, these peaks are around 402, 438 and 470 nm and are attributed to surface defects. In the doped samples the first peak showed slight blue shift whereas the second peak showed red shift which could be attributed to small variations in the complex trap/defect structures in nanoparticles. However, the third peak (470 nm) showed considerable red shift which increased with increasing Ni concentration extending up to 507 nm in the green region. This shift is due to the incorporation of more Ni^{2+} ions into the ZnS host lattice as the Ni^{2+} concentration increases. Song et al. [24] reported that the Ni^{2+} ions in octahedral sites can show three luminescence bands usually in the green, red and near infrared region but no emission is expected from Ni^{2+} in tetrahedral sites. Yang et al. [21] also reported a sharp strong green (520 nm) emission, with two fold enhancement in intensity from Ni^{2+} doped ZnS nanocrystals, which is assigned to the d–d optical transitions of Ni^{2+} luminescent center formed in ZnS. Murugadoss et al. [22] reported blue (470 nm) and green (498 nm) emissions from Ni doped ZnS nanoparticles and attributed these to the recombination between shallow donor levels and to the $^3T_2 \rightarrow {}^3A_2$ transition

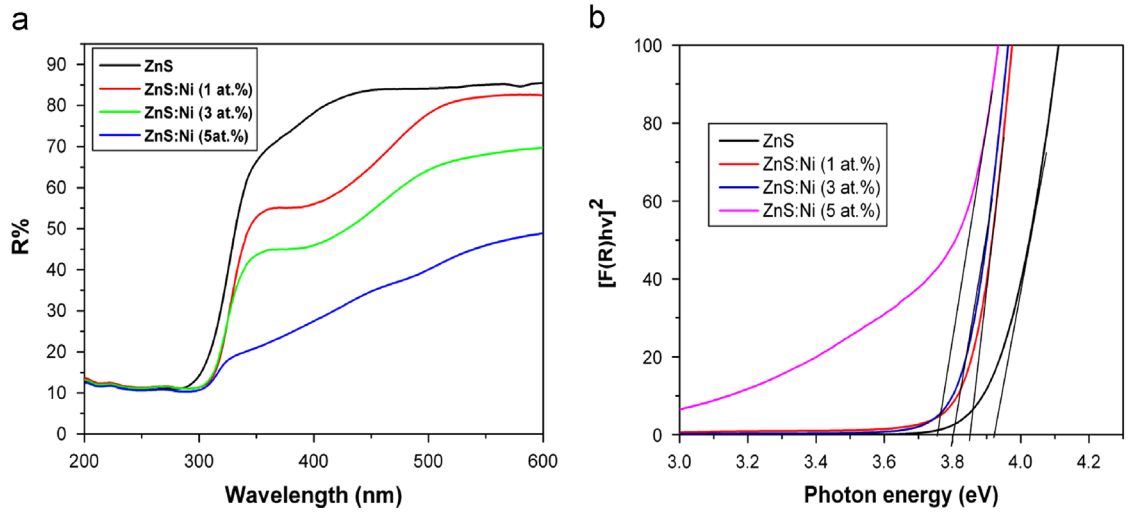

Fig. 4. (a) DRS spectra of ZnS:Ni (0, 1, 3 and 5 at%) nanoparticles and (b) Kubelka–Munk plots for band gap energy estimation of ZnS:Ni nanoparticles.

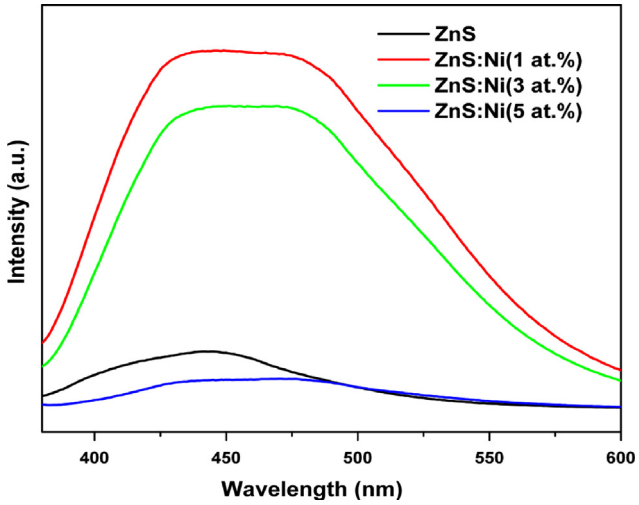

Fig. 5. PL spectra of ZnS:Ni (0, 1, 2, and 5 at%) nanoparticles.

of Ni^{2+} ions, respectively. Others [25,26] have reported that $^3T_2 \rightarrow {}^3A_2$ transition in tetrahedral Ni^{2+} gives rise to emission in the near infrared region. Bhorse et al. [20] observed only blue emission (425 nm) from Ni doped ZnS nanoparticles and reported PL quenching with increase in dopant concentration. Recently, Kumar et al. [14] also reported blue and green emissions in doped ZnS nanoparticles which were assigned to recombination between the shallow donor level (S vacancy) and the t_2 level of Ni^{2+} ions that replaced Zn^{2+} in the ZnS matrix. Thus the emission mechanism in tetrahedral Ni^{2+} appears to be complex and the picture is very confusing. Although the green emission observed in octahedral Ni^{2+} [24], was attributed to $^1T_2$ (^1D) $\rightarrow {}^3A_2$ (^3F) transition, the green emission observed by earlier authors [14,22,25,26], presumed to be from tetrahedral Ni^{2+}, could not be convincingly explained. On the other hand Balti et al. [23] assigned the green emission observed from substitutional ZnNiO nanoparticles to $^3T_2 \rightarrow {}^3A_2$ transition of Ni^{2+} ions in octahedral sites. These authors [23] speculated that this could be possible because some of the Ni^{2+} ions might have entered the octahedral (interstitial) sites of the host lattice. In the present Ni^{2+} doped ZnS nanoparticles, the Ni^{2+} ions have tetrahedral symmetry, since Ni^{2+} has an ionic radius of 0.69 Å which is less than that of Zn^{2+} (0.74 Å) and the XRD studies also indicate the formation of substitutional ZnNiS. Thus to conclude, we strongly believe that the broad emission band (covering blue to green) observed in the present doped samples may in fact be only related to the emissions from intrinsic ZnS nanoparticles and may not be from Ni^{2+} ions. The shift in the emission wavelength from blue to green with increasing Ni^{2+} doping may be attributed to modifications in the surface defect structure and the positions of the traps, shifting from shallow to deep levels below the edge of the conduction band, brought about by the increase in dopant concentration.

3.5. XPS analysis

Fig.7 shows the representative XPS spectrum of ZnS:Ni (5 at%) sample. The position of $2p_{3/2}$ and Zn $2p_{1/2}$ peak values related to Zn are at 1022.0 eV and 1044.2 eV respectively. It is obvious that the two spectra of Zn show symmetric single peaks, confirming that Zn exists mainly in +2 chemical state. The binding energy of the S 2p is 161.7 eV. It should be noted that the characteristic peak of Ni is not as strong as those of the other elements, showing that Ni is doped into the interior of the nanoparticles. Further, the peaks at 854.12 eV and 871.23 eV correspond to the binding energies of Ni $2p_{3/2}$ and Ni $2p_{1/2}$, respectively, illustrating that the valance state of Ni ion is +2 in the nanoparticles and that Ni is successfully doped into the ZnS nanoparticles without any impurity phases within the detection limit of the instrument.

3.6. Magnetic studies

Magnetization was studied at room temperature by using a vibrating sample magnetometer (VSM) and the results are shown in Fig.8. The figure shows that ZnS (undoped) samples are diamagnetic whereas all the doped samples are ferromagnetic. It may be noted from the figure that all the Ni doped

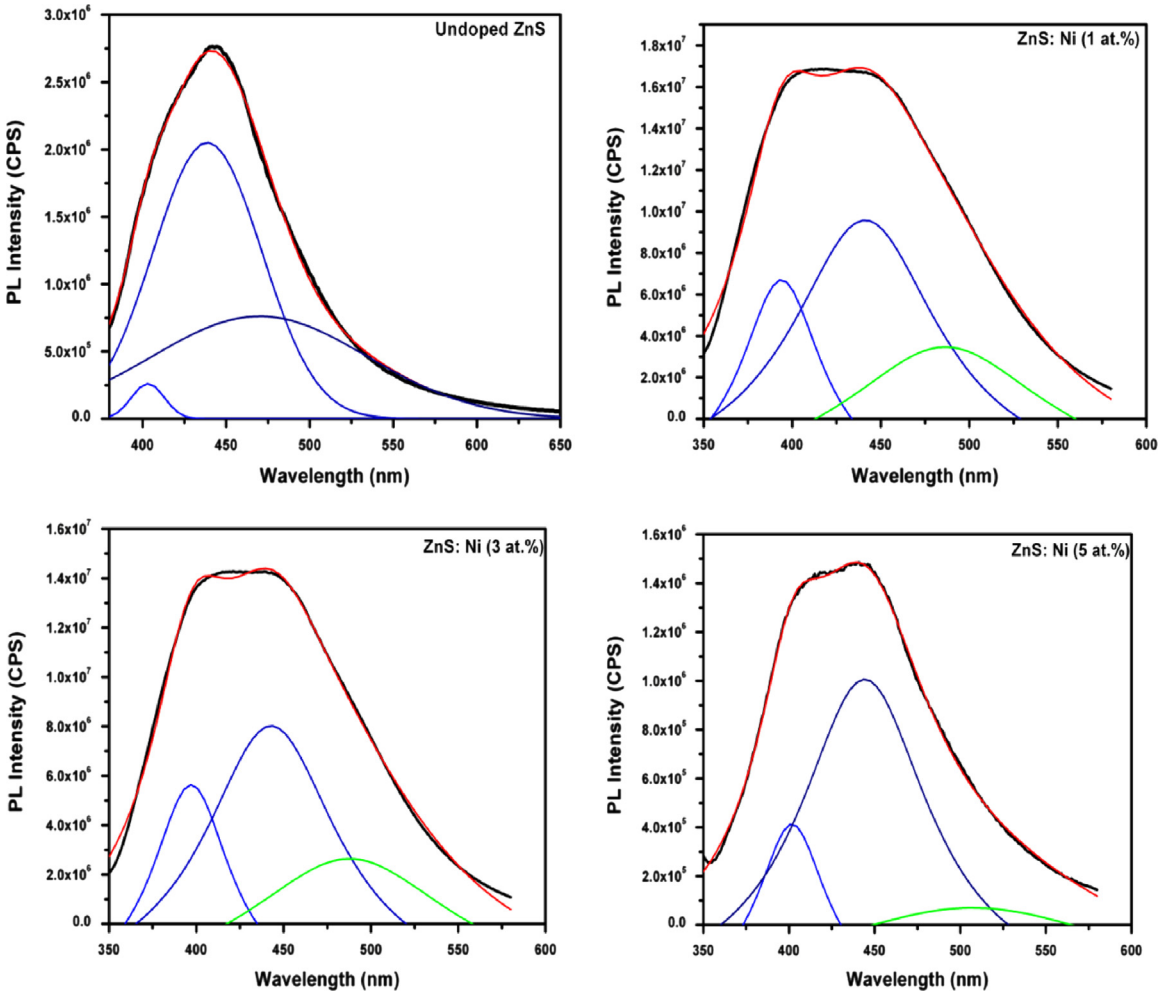

Fig. 6. Gaussian fit of PL data of ZnS:Ni (0, 1, 3 and 5 at%) nanoparticles.

samples exhibit magnetic hysteresis loops (M–H curves) indicating that all the doped samples are ferromagnetic with Curie temperature above room temperature. In 1 at% Ni doped samples, the magnetization curve indicates small hysteresis with low magnetization and coericivity with no saturation being observed. Also there appears to be a dominant diamagnetic contribution. Samples with 3 at% Ni exhibit a distinct hysteresis loop with magnetization attaining saturation. However, in samples doped with 5 at% Ni, although a distinct magnetic hysteresis is observed, magnetization has not attained saturation. Further, at higher applied fields the M–H curve appears to be linear with a definite slope indicating the presence of paramagnetic/superparamagnetic contributions to the magnetization [27]. This could be due to the presence of some nanoparticles of extremely small size [28] and also due to the presence of some impurity phases. The origin of ferromagnetism in DMS materials is still a subject of controversies. The observed ferromagnetism in transition metal doped ZnS has been attributed [29] to inclusion of impurity phases related to the dopant ion, to imperfections like grain boundaries. XRD patterns (Fig.2) and XPS (Fig.7) do not indicate the presence of either Ni clusters or any other impurity phases. This implies that either these are absent in the present

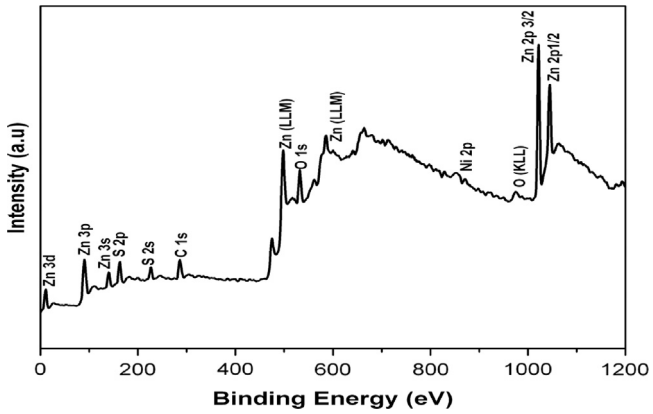

Fig. 7. XPS survey scan of ZnS:Ni (3 at%) nanoparticles.

samples or if present they are not within the detection limit of the instruments used. Formation of oxides and sulfides of Ni might be ruled out in the present samples as the samples were prepared at 80 °C. Even if they are present in minute quantities, they are reported to be either super paramagnetic or antiferromagnetic [30–32] and may not be responsible for the observed ferromagnetism of the present samples. In view of the

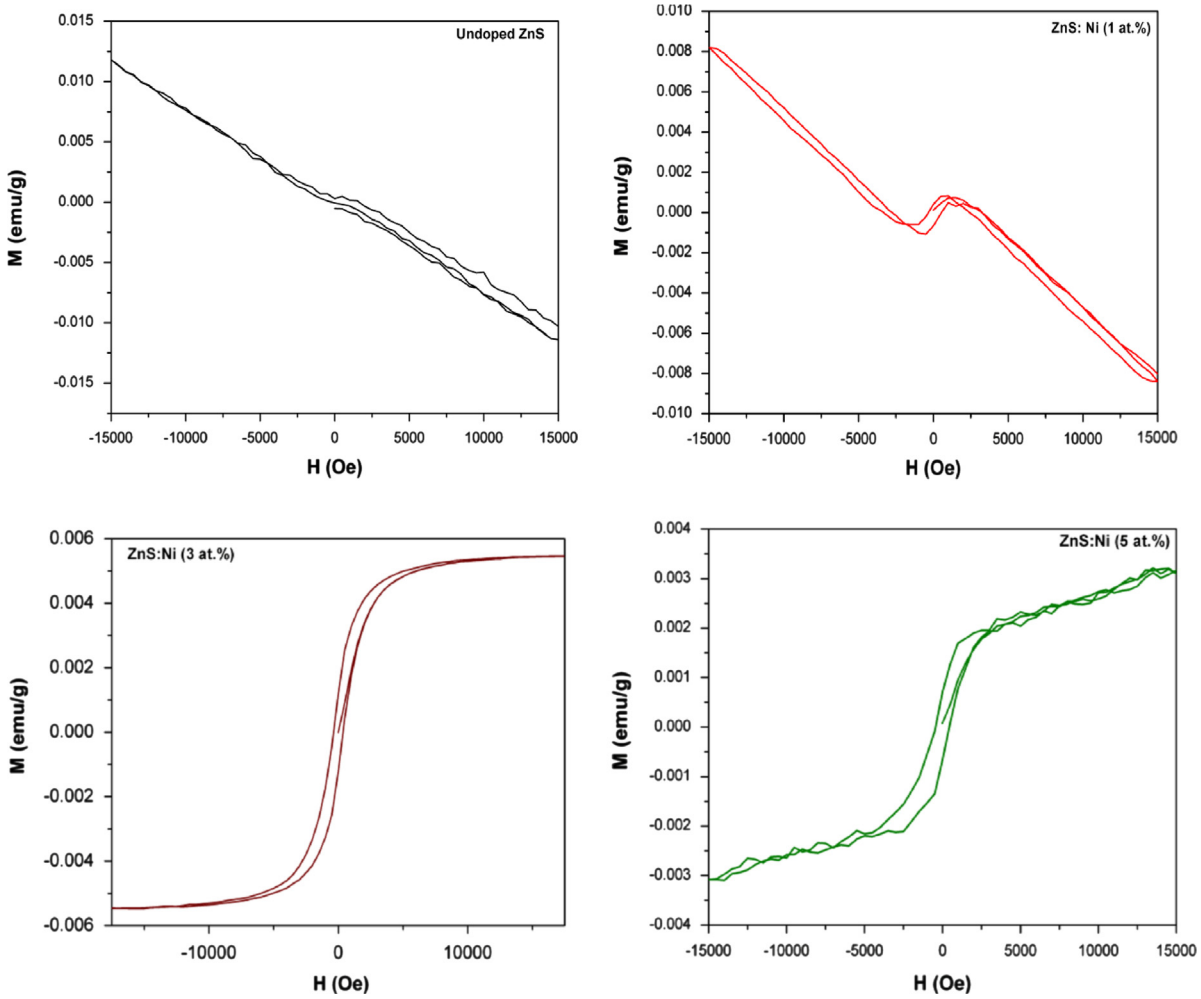

Fig. 8. M–H curves of ZnS:Ni (0, 1, 3 and 5 at%) nanoparticles.

Table1
Magnetization, coericivity and retentivity values for the ZnS:Ni (1, 3 and 5 at%) nanoparticles.

Nickel concentration (at%)	Magnetization (emu/g)	Coericivity (Gauss)	Retentivity (emu)
1	0.009	1375	21.613 E-6
3	0.107	361	1.1979 E-3
5	0.085	439	674.46 E-6

above factors, it is proposed that the ferromagnetism observed in the present Ni doped ZnS nanoparticles may be dopant induced and could originate from the long-range Ni^{2+}–Ni^{2+} ferromagnetic coupling mediated by shallow donor electrons [33]. This suggests that this could be carrier mediated ferromagnetism which is often reported [34] in DMS. Carrier mediated ferromagnetism in semiconductors depends on the magnetic dopant concentration as well as on the carrier type and carrier density. The values of magnetization, coericivity and retentivity for the present samples are given in Table1. The table indicates that the magnetization increases with increasing dopant concentration up to 3 at% of Ni. However, it drops for 5 at% Ni doped samples. In samples with lower concentration of Ni, the Ni ions are sufficiently far apart so that the indirect ferromagnetic coupling through the conduction electrons dominates over the direct antiferromagnetic coupling [35]. Hence, in samples with Ni concentration of 5 at% the magnetization decreases. This is because as the Ni doping increases, the Ni ions come closer to each other, which implies that Ni^{2+} ions have some Ni^{2+} ions as nearest neighbors. The super exchange interaction between these neighboring Ni^{2+} ions is antiferromagnetic in nature which brings down the magnetization. Also this could be due to the presence of a paramagnetic contribution to the magnetization as already mentioned. The present study indicates that the optimum doping level of Ni^{2+} in ZnS nanoparticles is around 3 at% for enhanced room temperature ferromagnetism. However, recently Kumar et al. [14] reported a continuous decreasing trend in the saturation magnetization of Ni doped ZnS nanoparticles with increasing dopant concentration in the entire range of composition [1–5 at%] studied.

4. Conclusions

In summary, the structural, optical and magnetic properties of ZnS:Ni (Ni = 0, 1, 3 and 5 at%) nanoparticles synthesized by refluxing technique at 80 °C were investigated. No secondary phase, apart from substitutional ZnNiS, was observed in

the XRD patterns in the whole range of composition studied. TEM studies suggest the formation of nanometric particles with average particle sizes in the range of 5–10 nm. The Ni dopant was well doped into the ZnS;Ni nanoparticles, as confirmed by XPS. Reflectance measurements showed a red shift in the optical absorption band edge indicating a decrease in band gap with increasing Ni concentration. All the doped samples showed broad and asymmetric PL peaks with dramatic increase in intensity compared to undoped samples. Gaussian fitting of the PL curves resulted in three deconvoluted peaks corresponding to blue and green emissions which are attributed to Ni dopant induced modifications of emissions characteristic of intrinsic ZnS nanoparticles. All the Ni doped ZnS nanoparticles exhibited carrier mediated ferromagnetism at room temperature. The present study indicates that the optimum doping levels of Ni in ZnS nanoparticles to observe enhanced PL intensity and enhanced room temperature ferromagnetism are 1 at% and 3 at%, respectively. The study suggests the application of this system in luminescent and new generation spintronic devices.

Acknowledgments

The authors are highly grateful to the University Grants Commission, New Delhi, India, for providing financial support. The authors are thankful to Mr. N. Sivaramakrishnan and Mr. Muthukumaran, SAIF, IIT Madras, Chennai for extending the VSM facility and to Dr. B. Sridhar, IICT, Hyderabad for doing the XPS studies.

References

[1] S.A. Wolf, D.D. Awschalom, R.A. Buhrman, J.M. Daughton, S.V. Molnar, M.L. Roukes, A.Y. Chtchelkanova, D.M. Treger, Spintronics: a spin-based electronics vision for the future, Science 294 (2001) 1488–1495.

[2] H. Ohno, Making non magnetic semiconductors ferromagnetic, Science 281 (1998) 951–956.

[3] S. Sambasivam, D. Paul Joseph, J.G. Lin, C. Venkateswaran, Doping induced magnetismin Co–ZnS nanoparticles, J. Solid State Chem. 182 (2009) 2598–2601.

[4] D. Amaranatha Reddy, G. Murali, R.P. Vijayalakshmi, B.K. Reddy, Room-temperature ferromagnetism in EDTA capped Cr-doped ZnS nanoparticles, Appl. Phys. A 105 (2011) 119–124.

[5] A.A. Dakhel, M. El-Hilo, Ferromagnetic nanocrystalline Gd-doped ZnO powder synthesized by coprecipitation, J. Appl. Phys. 107 (2010) 123905.

[6] J.H. Zheng, J.L. Song, Z. Zhao, Q. Jiang, J.S. Lian, Optical and magnetic properties of Nd-doped ZnO nanoparticles, Cryst. Res. Technol. 47 (2012) 713–718.

[7] M. Venkatesan, C.B. Fitzgerald, J.M.D. Coey, Thin films: unexpected magnetism in adielectric oxide, Nature 430 (2004) 630.

[8] M.H.F. Sluiter, P.K. Sharma, A. Inoue, A.R. Raju, C. Rout, U.V. Waghmare, First principles based design and experimental evidence for a ZnO-based ferromagnet at room temperature, Phys. Rev. Lett. 94 (2005) 187204.

[9] R.N. Bhargava, D. Gallagher, X. Hong, A. Nurmikko, Optical properties of manganese-doped nanocrystals of ZnS, Phys. Rev. Lett. 72 (1994) 416–419.

[10] S. Sambasivam, B. Sathyaseelan, D. Raja Reddy, B.K. Reddy, C.K. Jayasankar, ESR and photoluminescence properties of Cu doped ZnS nanoparticles, Spectrochim. Acta A 71 (2008) 1503–1506.

[11] D. Amaranatha Reddy, A. Divya, G. Murali, R.P. Vijayalakshmi, B.K. Reddy, Synthesis and optical properties of Cr doped ZnS nanoparticles capped by 2-mercaptoethanol, Physica B 406 (2011) 1944–1949.

[12] X. Jia, M. Qin, W. Yang, Magnetism in Cr-doped ZnS: density-functional theory studies, J. Phys. D: Appl. Phys. 42 (2009) 235001.

[13] S. Sambasivam, D. Paul Joseph, D. Raja Reddy, B.K. Reddy, C.K. Jayasankar, Synthesis and characterization of thiophenol passivated Fe-doped ZnS nanoparticles, Mater. Sci. Eng. B 150 (2008) 125–129.

[14] S. Kumar, C.L. Chen, C.L. Dong, Y.K. Ho, J.F. Lee, T.S. Chan, R. Thangavel, T.K Chen, B.H. Mok, S.M. Rao, M.K. Wu, Room temperature ferromagnetism in Ni dopedZnS nanoparticles, J. Alloys Compd. 554 (2013) 357–362.

[15] A.K. Singh, Advanced X-ray Techniques in Research and Industries, IOS, India, 2005.

[16] A. Escobedo Morales, E. Sanchez Mora, U. Pal, Use of diffuse reflectance spectroscopy for optical characterization of un-supported nanostructures, Rev. Mex. Fis. S 53 (2007) 18–22.

[17] S. Colis, H. Bieber, S.B. Colin, G. Schmerber, C. Leuvrey, A. Dinia, Magnetic propertiesof Co-doped ZnO diluted magnetic semiconductors prepared by low-temperature mechanosynthesis, Chem. Phys. Lett. 422 (2006) 529–533.

[18] A. Bouaine, N. Brihi, G. Schmerber, C.U. Bouillet, S. Colis, A. Dinia, Structural,optical, and magnetic properties of co-doped SnO_2 powders synthesized by the coprecipitation technique, J. Phys. Chem C 111 (2007) 2924–2928.

[19] V. Ramasamy, K. Praba, G. Murugadoss, Study of optical and thermal properties in nickel doped ZnS nanoparticles using surfactants, Superlattices Microstruct. 51 (2012) 699–714.

[20] P.H. Borse, N. Deshmukh, R.F. Shinde, S.K. Date, S.K. Kulkarni, Luminescence quenching in ZnS nanoparticles due to Fe and Ni doping, Mater. Sci. 34 (1999) 6087–6093.

[21] P. Yang, M. Lu, D. Xu, D. Yuan, J. Chang, G. Zhou, M. Pan, Strong green luminescenceof Ni^{2+}-doped ZnS nanocrystals, Appl. Phys. A 74 (2002) 257–259.

[22] G. Murugadoss, M. Rajesh Kumar, Synthesis and optical properties of monodispersed Ni^{2+}-doped ZnS nanoparticles, Appl. Nanosci. (2012).

[23] I. Balti, A. Mezni, A.D. Omrani, P. Leone, B. Viana, O. Brinza, L.S. Smiri, N. Jouini, Comparative study of Ni- and Co-substituted ZnO nanoparticles: synthesis, optical, and magnetic properties, J. Phys. Chem. C 115 (2011) 15758–15766.

[24] C.F. Song, M.K. Lu, F. Gu, S.W. Liu, S.F. Wang, D. Xu, D.R. Yuan, Effect of Al^{3+} on the photoluminescence properties of Ni^{2+}-doped sol–gel SiO_2 glass, Inorg. Chem. Commun. 6 (2003) 523–526.

[25] T. Suzuki, G.S. Murugan, Y. Ohishi, Optical properties of transparent Li_2O–Ga_2O_3–SiO_2 glass-ceramics embedding Ni-doped nanocrystals, Appl. Phys. Lett. 86 (2005) 131903.

[26] B. Wu, S. Zhou, J. Ruan, Y. Qiao, D. Chen, C. Zhu, J. Qiu, Enhanced near-infrared emission from Ni^{2+} in Cr^{3+}/Ni^{2+} codoped transparent glass ceramics, Appl. Phys. Lett. 92 (2008) 151102.

[27] Paul R Kelso, Basil Tikoff, Mike Jackson, W. Sun, A new method for the separation of paramagnetic and ferromagnetic susceptibility anisotropy using low field and high field methods, Geophys. J. Int. 151 (2002) 345–359.

[28] I.V. Beketov, A.P. Safronov, A.I. Medvedev, J. Alonso, G.V. Kurlyandskaya, S.M Bhagat, Iron oxide nanoparticles fabricated by electric explosion of wire: focus on magnetic nanofluids, AIP Adv. 2 (2012) 022154.

[29] S.P. Patel, J.C. Pivin, A.K. Chawla, R. Chandra, D. Kanjilal, L. Kumar, Room temperature ferromagnetism in $Zn_{1-x}Co_xS$ thin films with wurtzite structure, J. Magn. Magn. Mater. 323 (2011) 2734–2740.

[30] M. Ghosh, K. Biswas, A. Sundaresan, C.N.R. Rao, MnO and NiO nanoparticles: synthesis and magnetic properties, J. Mater. Chem. 16 (2006) 106–111.

[31] M.S. Niasari, F. Davar, M. Mazaheri, Synthesis, characterization and magnetic propertiesof NiS_{1+x} nanocrystals from [bis (salicylidene) nickel (II)] as new precursor, Mater. Res. Bull. 44 (2009) 2246–2251.

[32] C. Schuster, M. Gatti, A. Rubio, Electronic and magnetic properties of NiS_2, NiSSe and $NiSe_2$ by a combination of theoretical methods, Eur. Phys. J. B 85 (2012) 325.

[33] J.M.D. Coey, M. Venkatesan, C.B. Fitzgerald, Donor impurity band exchange in dilute ferromagnetic oxides, Nat. Mater. 4 (2005) 173–179.

[34] G.J. Huang, J.B. Wang, X.L. Zhong, G.C. Zhou, H.N. Yan, Synthesis, structure, and room-temperature ferromagnetism of Ni-doped ZnO nanoparticles, J. Mater. Sci. 42 (2007) 6464–6468.

[35] I. Djerdj, Z. Jaglicic, D. Arcon, M. Niederberger, Co-doped ZnO nanoparticles: mini review, Nanoscale 2 (2010) 1096–1104.